Supporting Information for

Co-engineering of Fe-Mn nanocluster with porous carbon for enhanced electrocatalytic ammonia synthesis

Youqing Wang[a], Lang Zhang[a], Caiyun Wang[b], Zhiwei Wang[a], Yanhong Feng[a]*, and Xijun Liu[a]*4*

a) *MOE Key Laboratory of New Processing Technology for Nonferrous Metals and Materials, School of Resources, Environment and Materials, Guangxi University, Nanning, 530004 Guangxi, China. E-mail: fyh0811@gxu.edu.cn; xjliu@gxu.edu.cn.*
b) *Guangxi Vocational & Technical Institute of Industry, Nanning 530001, China. E-mail: wangcaiyun@gxgy.edu.cn*

Materials

Ar was purchased from Nanning Air Gas Co., Ltd (China). Citric acid monohydrate ($C_6H_8O_7$•H_2O) and hydrofluoric acid (HF) were purchased from Sinopharm Group Chemical Reagent Co., Ltd (China). Silicon dioxide (SiO_2), iron nitrate nonahydrate ($Fe(NO_3)_3$•$9H_2O$), ammonium chloride (NH_4Cl), potassium nitrate (KNO_3) and potassium sulfate anhydrous (K_2SO_4) were purchased from Shanghai Aladdin Co., Ltd (China). Manganese(Ⅱ) nitrate tetrahydtate ($Mn(NO_3)_2$•$4H_2O$) was purchased from Macklin Reagent Company. Deuterated dimethyl sulfoxide (DMSO-d_6) analytical grade purchased from Innochem. The aqueous solution used in the experiment was prepared from H20PRO-VF water purification system.

Synthesis of NC-Fe_xMn_y/NOPC

Take NC-Fe_1Mn_2/NOPC for example, a solution was prepared by dissolving 5.0 g of $C_6H_8O_7$•H_2O , 5.0 g of NH_4Cl, 1.5 g of SiO_2, 0.17 g $Fe(NO_3)_3$·$9H_2O$, and 0.21 g $Mn(NO_3)_2$•$4H_2O$ in 15 mL of deionized water using ultrasonication and magnetic stirring. The homogeneous solution was subsequently freeze-dried in a vacuum to obtain a solid mixtures which was then grounding about 10 min to obtain a well-mixed reactant powder. The powder was carbonized at a temperature of 900ºC for 3 hours under an Ar atmosphere with a heating rate of 10 ºC min^{-1}. Finally, the resulting black product was treated with HF (5 wt%) at room temperature to remove the SiO_2 template followed by washing and drying to obtain NC-Fe_1Mn_2/NOPC. The synthesis steps of NC-Fe_xMn_y/NOPC

(x:y = 4:1, 2:1, 1:1, and 1:4) are the same, but replace the masses of Fe and Mn to 0.4 g $Fe(NO_3)_3·9H_2O$ and 0.06 g $Mn(NO_3)_2•4H_2O$ (4:1), 0.33 g $Fe(NO_3)_3·9H_2O$ and 0.1 g $Mn(NO_3)_2•4H_2O$ (2:1), 0.25 g $Fe(NO_3)_3·9H_2O$ and 0.16 g $Mn(NO_3)_2•4H_2O$ (1:1), 0.1 g $Fe(NO_3)_3·9H_2O$ and 0.25 g $Mn(NO_3)_2•4H_2O$ (1:4) respectively. It is worth noting that the definition of 'Fe_xMn_y' is based on the following: Taking 'Fe_1Mn_2' as an example, during synthesis, a total mass of 0.5 g of Fe-containing material is used as a standard to determine the amount of substance (n); one third of n is used to find the mass of the Fe-containing material, while two thirds of n is replaced by the Mn-containing material to find the mass of the Mn-containing material. Therefore, 'Fe_1Mn_2' is theoretically defined as a molar ratio of Fe to Mn of 1:2 during synthesis.

Synthesis of NC-Mn/NOPC

The synthesis steps for NC-Fe/NOPC are the same as for NC-Fe_1Mn_2/NOPC. Replace 0.17 g $Fe(NO_3)_3·9H_2O$, and 0.21 g $Mn(NO_3)_2•4H_2O$ with 0.5 g of $Fe(NO_3)_3·9H_2O$.

Synthesis of NC-Mn/NOPC

The synthesis steps for NC-Mn/NOPC are the same as for NC-Fe_1Mn_2/NOPC. Replace 0.17 g $Fe(NO_3)_3·9H_2O$, and 0.21 g $Mn(NO_3)_2•4H_2O$ with 0.31 g of F $Mn(NO_3)_2•4H_2O$.

Material characterizations

The morphology of catalysts was investigated by field emission Scanning electron microscopy (SEM, ZEISS VLTRA-55) and transmission electron

microscopy (TEM, FEI Tecnai G2 F20). The Raman spectra were acquired on a Renishaw in via Raman microscope with the 532 nm laser. X-ray diffraction (XRD) measurements were performed on a D8ADVANCE X-ray diffractometer (Bruker). The X-ray photoelectron spectroscopy (XPS) analyses were performed with an ESCALAB 250 Xi X-ray photoelectron spectrometer. The Nuclear magnetic resonance (NMR) spectra were measured on an Ascend 600 MHz NMR spectrometer (Bruker).

NO_3RR tests

All electrochemical characterizations were conducted using a CHI 760E workstation integrated with a three-electrode configuration within a two-compartment cell, which was divided by a Nafion 117 membrane. The catalyst loading on the carbon paper (Hesen, HCP-020), the graphite rod and the Ag/AgCl (saturated KCl solution) were applied as working electrode, counter electrode and reference electrode, respectively. The single reaction (NO_3RR) was tested in an H-type cell with 0.1 M KNO_3 and 0.1 M K_2SO_4 electrolyte. The produced NH_3 in electrolytes was quantified using UV-Vis spectrometer (Shimadzu UV-2700). All applied potentials in this work have been converted to the RHE scale. The testing range was from −0.7 V (vs. RHE) to −1.6 V (vs. RHE). The concentration of ammonium ions in the reacted electrolyte was determined using the indophenol blue method to calculate the Faradaic efficiency.

Zn-NO_3^- battery performance

The NC-Fe_1Mn_2/NOPC (1 cm^2) and Zn plate (3 cm^2) were used as the cathode and anode, respectively. The anolyte was 1 M KOH and the catholyte was 0.1 M KNO_3 and 0.1 M K_2SO_4. A bipolar membrane was employed to separate the two chambers.

Computational Method

In this study, a series of density functional theory (DFT) calculations were performed using an advanced ab initio simulation software package.[1] To handle electronic exchange and correlation effects, the Perdew-Burke-Ernzerhof (PBE) exchange-correlation functional based on the generalized gradient approximation (GGA) was chosen.[2, 3] The kinetic energy cutoff was set to 450 eV to ensure the accuracy of energy convergence. All computational models used a 1 × 1 × 1 k-point mesh to sample the Brillouin zone to achieve the desired computational precision. At the same time, an appropriate vacuum region (e.g., 15 Å) was introduced in the Z-axis direction to reduce interactions between periodic images. The convergence threshold for electronic self-consistent calculations was strictly set to 10^{-5} eV, while the convergence criterion for ionic relaxation was set to 0.05 eV/Å.

The free energy change (ΔG) for each adsorbed intermediate is calculated using the following expression:

$$\Delta G = \Delta E + \Delta EZPE - T\Delta S$$

Where ΔE, ΔEZPE, and ΔS represent the changes in electronic energy, zero-point energy, and entropy associated with the adsorption of the intermediate,

respectively. The thermodynamic corrections at the reaction temperature (298 K) were calculated using the NIST database (NIST Standard Reference Database 13, Last Update to Data Content: 1998. DOI: 10.18434/T42S31 https://janaf.nist.gov/).

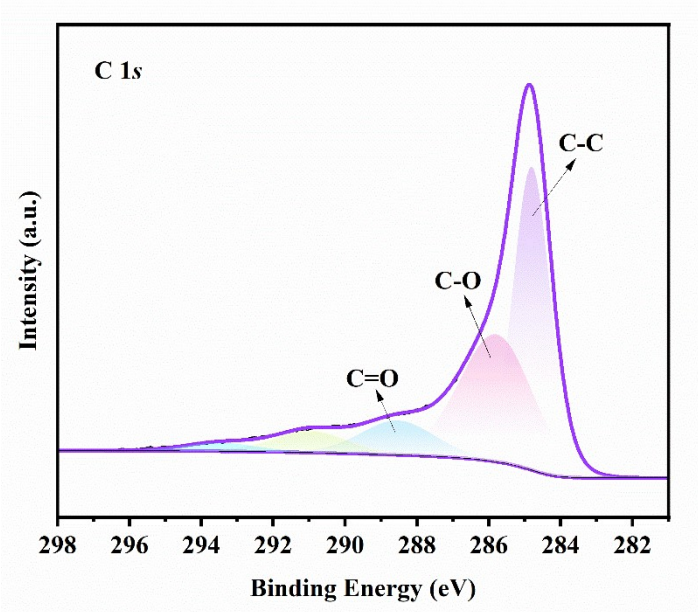

Figure S1. C 1s XPS spectra of NC-Fe_1Mn_2/NOPC sample.

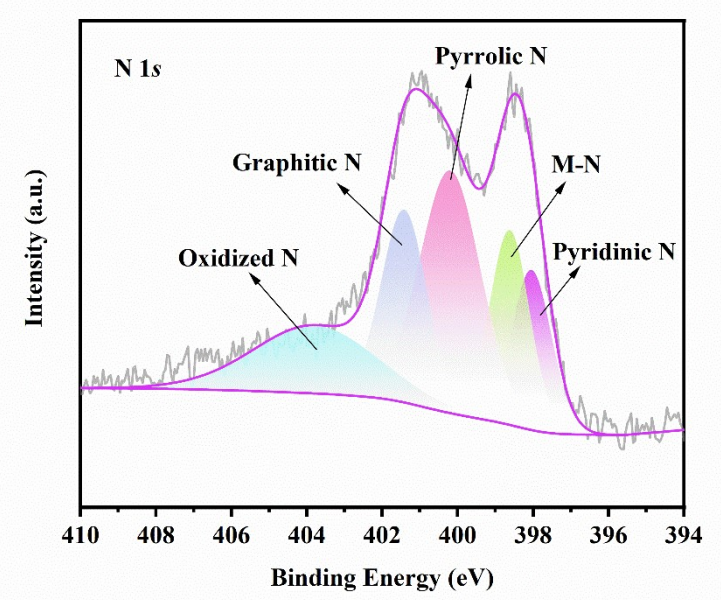

Figure S2. N 1s XPS spectra of NC-Fe_1Mn_2/NOPC sample.

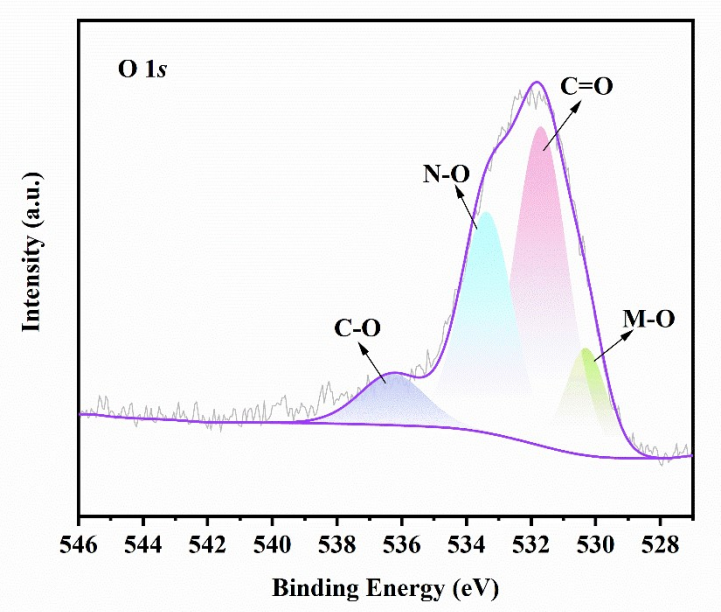

Figure S3. O 1s XPS spectra of NC-Fe_1Mn_2/NOPC sample.

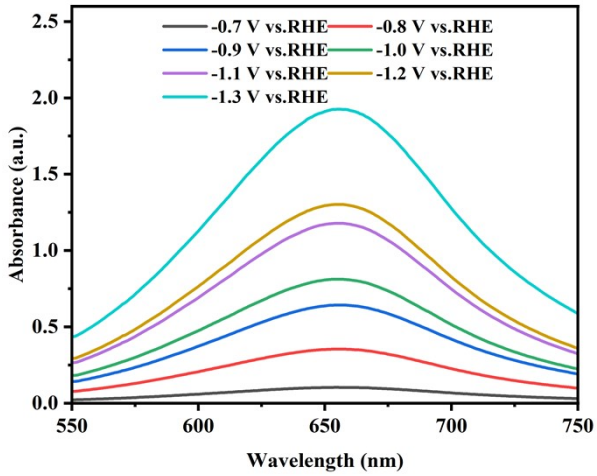

Figure S4. The UV/Vis absorption spectra of the NC-Fe_1Mn_2/NOPC.

.

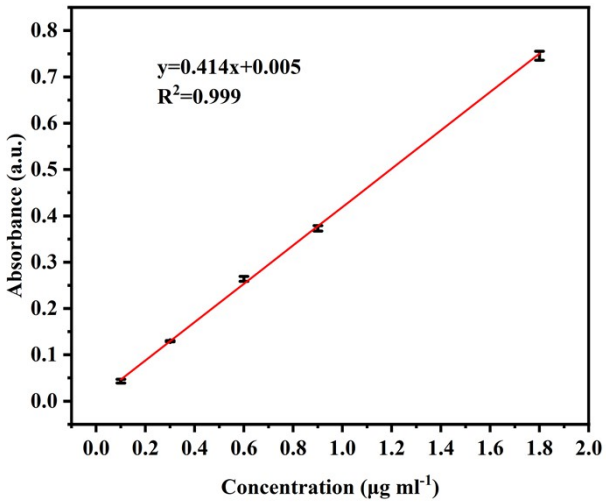

Figure S5. The calibration curve used to estimate the NH_3 yield and FE.

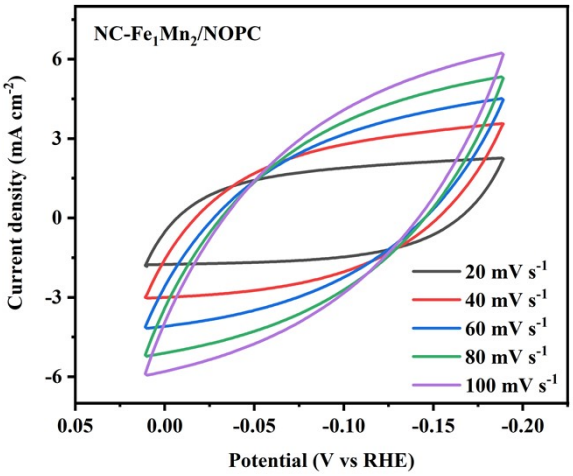

Figure S6. The CV curves of NC-Fe_1Mn_2/NOPC at different scan rates.

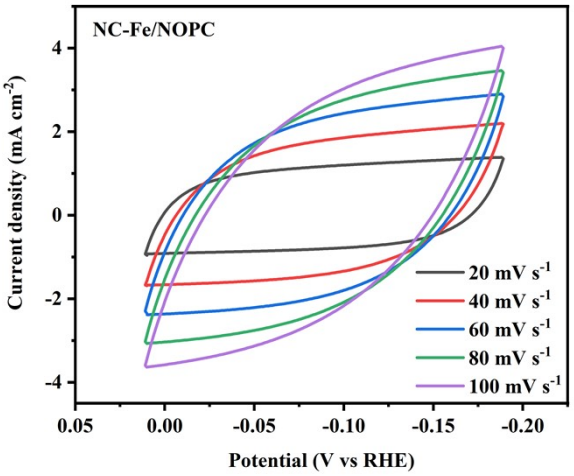

Figure S7. The CV curves of NC-Fe/NOPC at different scan rates.

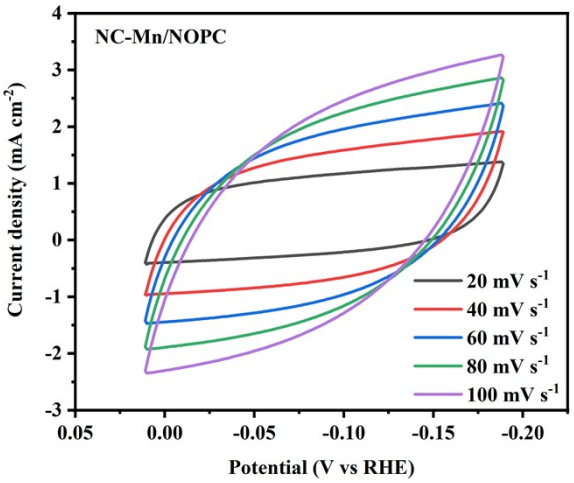

Figure S8. The CV curves of NC-Mn/NOPC at different scan rates.

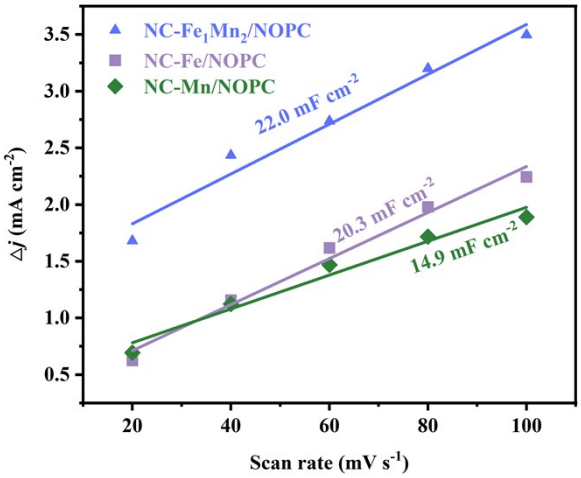

Figure S9. Electrochemical surface areas of the NC-Fe_1Mn_2/NOPC, NC-Fe/NOPC, and NC-Mn/NOPC.

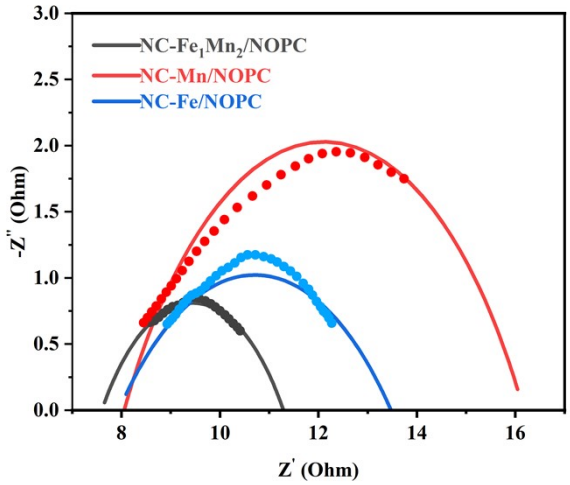

Figure S10. Electrochemical impendence spectra of the NC-Fe_1Mn_2/NOPC, NC-Fe/NOPC, and NC-Mn/NOPC.

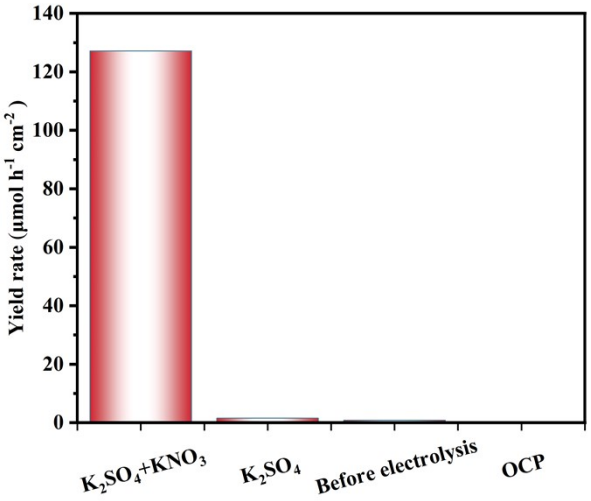

Figure S11. NH_3 yield rate comparison under different conditions.

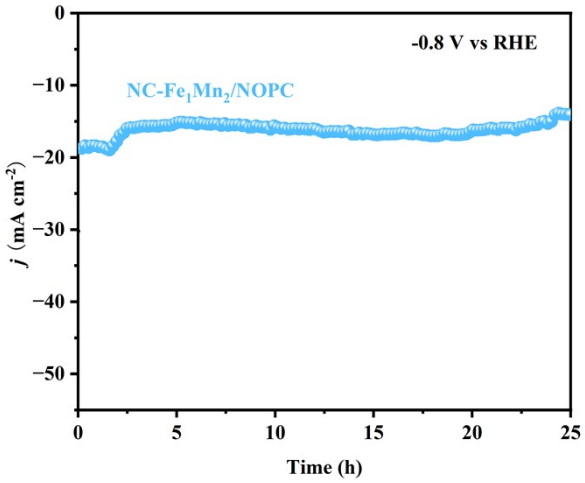

Figure S12. Chronoamperometry stability test at a potential of –0.8 V vs RHE.

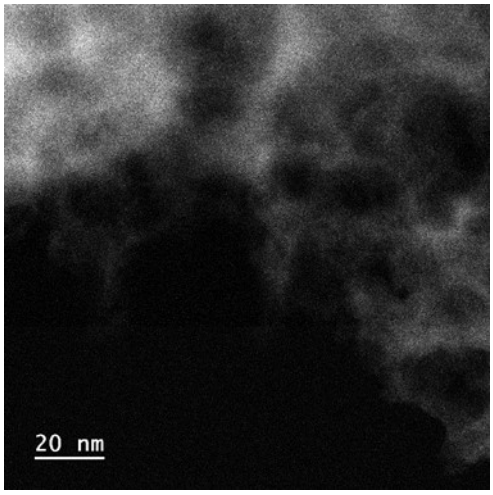

Figure S13. TEM image of NC-Fe_1Mn_2/NOPC after stability test.

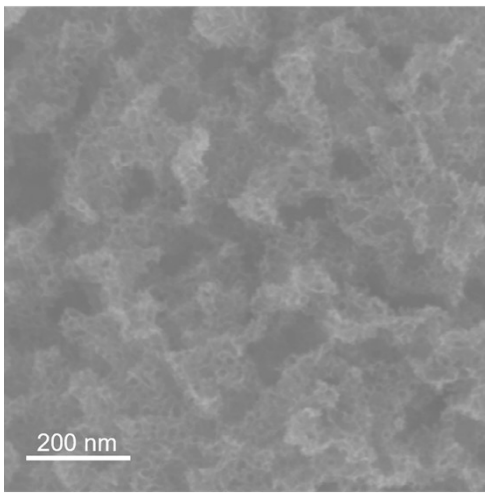

Figure S14. SEM image of NC-Fe_1Mn_2/NOPC after stability test.

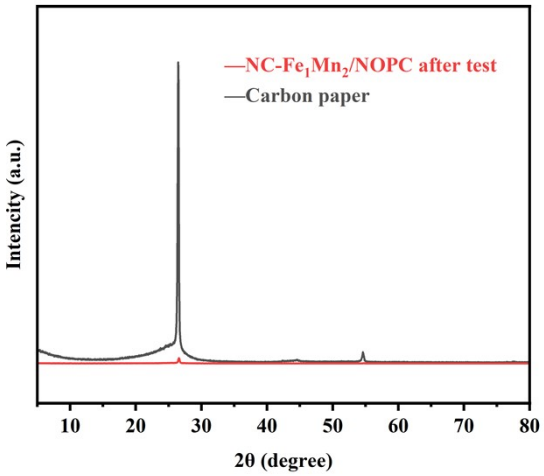

Figure S15. XRD patterns of NC-Fe_1Mn_2/NOPC after stability test. Clearly, no additional peaks can be observed after the stability test.

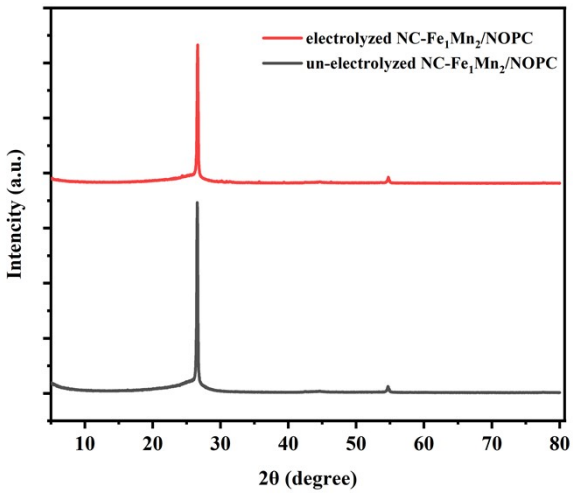

Figure S16. XRD patterns of un-electrolyzed NC-Fe_1Mn_2/NOPC before stability test and electrolyzed NC-Fe_1Mn_2/NOPC after stability test.

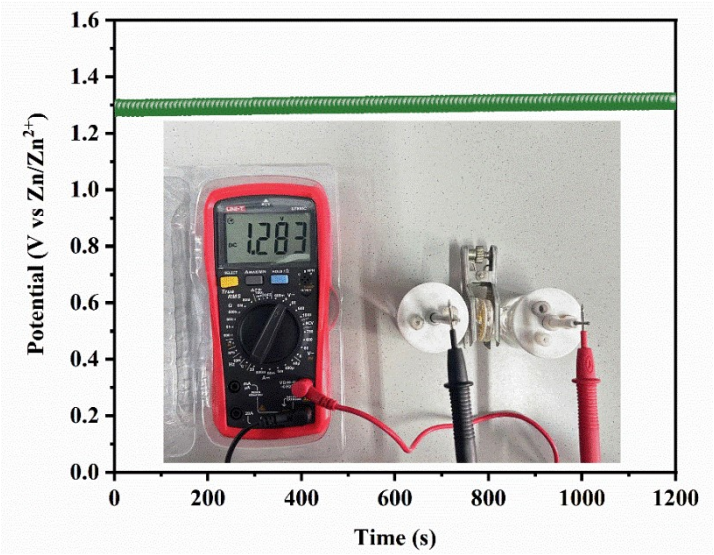

Figure S17. OCP of the Zn-NO_3^- battery with the NC-Fe_1Mn_2/NOPC cathode.

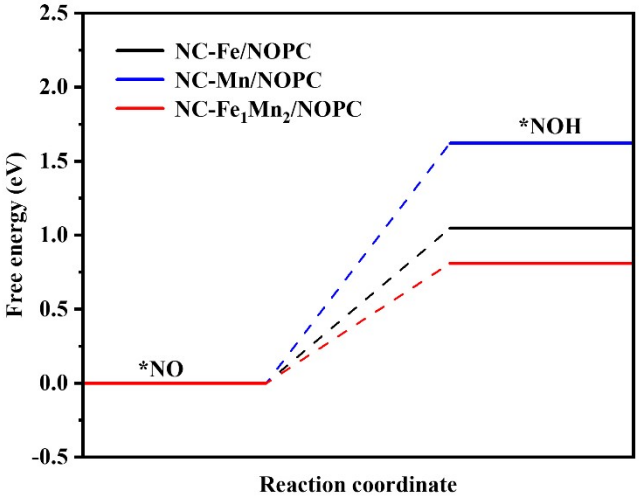

Figure S18. Free energy diagrams for NO_3RR on NC-Fe/NOPC, NC-Mn/NOPC and NC-Fe_1Mn_2/NOPC. According to the literature[4,5], the potential-determining step of NO_3RR on transition metal-based clusters is correspond to the formation of *NOH. In this case, the free energy of the transformation of *NO to *NOH of NC-Fe_1Mn_2/NOPC is the lowest (0.8 eV) in comparison to those of NC-Fe/NOPC (1 eV), NC-Mn/NOPC (1.62 eV), which means that the synergistic effect of Fe and Mn conducive to improving the selectivity of NO_3RR.

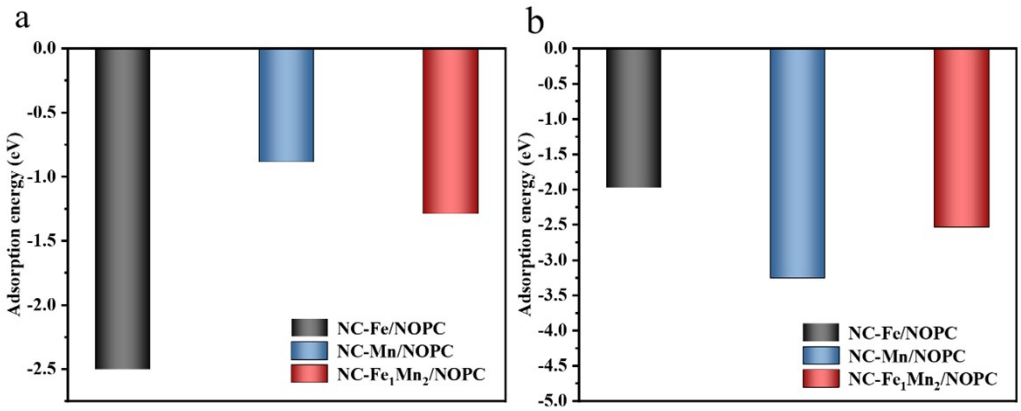

Figure S19. Comparison of (a) H adsorption energy and (b) NO_3^- adsorption energy of NC-Fe/NOPC, NC-Mn/NOPC and NC-Fe_1Mn_2/NOPC. As shown in Figure S19a, the doping of Fe reduced the adsorption of H, weakened the competitive reaction of HER, and promoted the NO_3RR. Meanwhile, in Figure S19b, the addition of Fe enhanced the adsorption of NO_3^- and increases the adsorption energy.

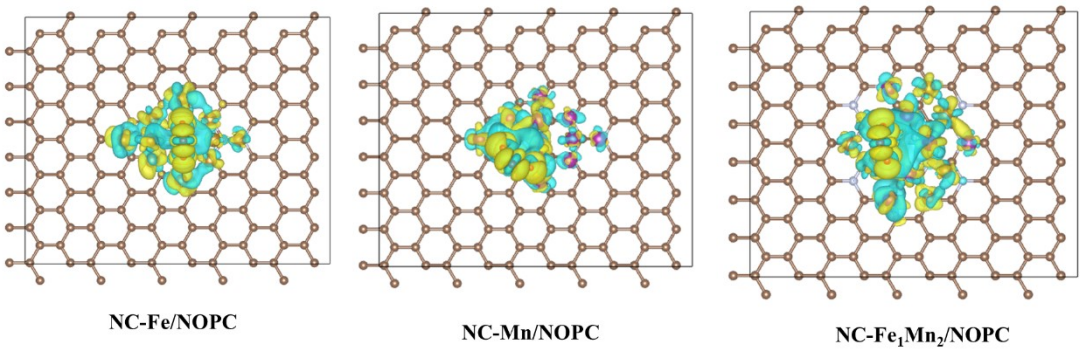

Figure S20. Charge density differences of NO_3^- on NC-Fe/NOPC, NC-Mn/NOPC and NC-Fe_1Mn_2/NOPC (Note that the yellow area represents the gained electrons, and the cyan area represents the lost electrons). The number of transferred electrons of NC-Fe/NOPC, NC-Mn/NOPC and NC-Fe_1Mn_2/NOPC can be obtained by calculating the Bader charges, which are 0.773, 0.776 and 0.787 respectively. It can be seen that the number of electrons gained and lost of Fe and Mn double doping catalyst is more than NC-Fe/NOPC and NC-Mn/NOPC, which means that the NC-Fe_1Mn_2/NOPC has stronger electron interaction.

Table S1. Electrocatalysis results from this work and those reported NO_3RR results in the literature.

Catalysts	NH_3 yield rate	FE(%)	Electrolyte	Ref.
R-Cu_2O/Cu/CF	2.17 mg h^{-1} cm^{-1}	84.36	1M KOH+250mg L^{-1} NO_3^-	[6]
Fe/Cu-HNG	1.08 mmol h^{-1} mg^{-1}	92.51	1M KOH+0.1M $^{15}NO_3^-$ or 0.1M $^{14}NO_3^-$	[7]
1D-2D CoPc_RGO	58.82 ug h^{-1} mg^{-1}	95.12	0.1M K_2SO_4+200 ppm KNO_3	[8]
Ce-MoS_{2-X}	7.3 mg h^{-1} cm^{-1}	96.6	0.5M Na_2SO_4+0.1M $NaNO_3$	[9]
Bi_1Pd	33.8 mg h^{-1} cm^{-1}	99.6	1M KOH+0.1M NO_3^-	[10]
Co_1-P/NPG	8.6 mg h^{-1} mg^{-1}	93.8	0.5M K_2SO_4+0.1M KNO_3	[11]
POVs-$Cu^{\delta+}$-TiO_2.	1321.2 umol h^{-1} cm^{-1}	95.0	1M KOH+0.1M ppm of NO_3^--N	[12]
NC-Fe_1Mn_2/NOPC	359.87 umol h^{-1} cm^{-1}	87.73	0.1M KNO_3+0.1M K_2SO_4	This work

Reference

[1]. G. Kresse; J. Hafner. *Physical review B* **1993**, 47, 558.
[2]. J. P. Perdew; K. Burke and Y. Wang. *Physical review B* **1996**, 54, 16533.
[3]. M. Krack. *Theoretical Chemistry Accounts* **2005**, 114, 145-152.
[4]. L. Xu, T. Liu, D. Liu, A. Xu, S. Wang, H. Huang, X. Liu, M. Sun, Q. Luo, X. Zheng, T. Ding, T. Yao, *Nano Lett.* **2024**, 24, 1197-1204.
[5]. T. Hou, T. Wei, Y. Wu, L. Zhang, J. Ding, Q. Liu, L. Feng, X. Liu, *J. Colloid Interface Sci.* **2024**, *674*, 834-840.
[6]. W. Fu; Z. Hu; Y. Zheng; P. Su; Q. Zhang; Y. Jiao; M. Zhou. *Chem. Eng. J.* **2022**, 433.
[7]. S. Zhang; J. Wu; M. Zheng; X. Jin; Z. Shen; Z. Li; Y. Wang; Q. Wang; X. Wang; H. Wei; J. Zhang; P. Wang; S. Zhang; L. Yu; L. Dong; Q. Zhu; H. Zhang; J. Lu. *Nat. Commun.* **2023**, 14, 3634.
[8]. S. Paul; S. Sarkar; A. Adalder; S. Kapse; R. Thapa; U. K. Ghorai. *ACS Sustainable Chem. Eng.* **2023**, 11, 6191-6200.
[9]. Y. Luo; K. Chen; G. Wang; G. Zhang; N. Zhang; K. Chu. *Inorg. Chem. Front.* **2023**, 10, 1543-1551.
[10]. K. Chen; Z. Ma; X. Li; J. Kang; D. Ma; K. Chu. *Adv. Funct. Mater.* **2023**, 33, 2209890.
[11]. J. Ni; J. Yan; F. Li; H. Qi; Q. Xu; C. Su; L. Sun; H. Sun; J. Ding; B. Liu. *Adv. Energy Mater.* **2024**, 14, 2400065.
[12]. L.-Y. Zhang; W. Shang; S. Qiao; W. Liu; Y. Shi. *ACS Catal.* **2024**, 14, 15827-15836.